Application of a detailed bin scheme in longwave radiation transfer modeling

Eszter Lábó[*][1] and **István Geresdi**[2]

[1]*Hungarian Meteorological Service,*
P.O. Box 38, H-1525 Budapest, Hungary

[2]*Szentagothai Research Center, University of Pécs,*
Ifjúság útja 20, H-7624 Pécs, Hungary

Corresponding author E-mail: labo.e@met.hu

Abstract—Absorption and transfer of radiation in clouds are sensitive to size distribution of water drops. A new numerical scheme has been developed for calculating the extinction coefficients of water clouds in the longwave region. While the generally applied bulk schemes in numerical models characterize the whole size distribution of the water droplets with one parameter (effective radius), detailed models allow us to calculate the optical properties without any assumption about the size distribution of water drops. Our model uses a bin microphysical scheme which uses the number concentration and mixing ratios of water in 36 size intervals.

This paper describes the developed bin radiation scheme. The wavelength-dependence of extinction coefficients calculated by bin and bulk schemes is compared at different effective radius. It was also investigated how the number concentration of droplets and liquid water content affect the difference between the two schemes. The relative difference depends both on the effective radius and on the wavelength. If the effective radius is larger than 10 μm, the relative difference remains below 20%. It is higher in the case of smaller effective radius.

The bin scheme has also been implemented in the RRTM LW radiation transfer model code. Upward, downward, and net radiation profiles for four different cases were studied with the RRTM model. It was found that the outgoing longwave radiation is sensitive on the applied scheme when the cloud layer is thin. Significant differences were found between the gradients of the net longwave radiation profiles in all cases. These differences have significant impact on the evolution of the vertical temperature profiles, which affects both cloud dynamics and microphysics.

Key-words: longwave radiation, bin scheme, numerical modeling, cloud-radiation interaction, water clouds, cooling rate

1. Introduction

The large impact of clouds on the temperature profiles and radiation budget stirs the need for a more accurate modeling of cloud-radiation interactions (*Ramanathan* and *Inamdar,* 2006; *Corti* and *Peter,* 2009). Recent research focuses on the development of more precise calculation methods of radiative cloud forcing (*Liu et al.,* 2009). Besides models, measurement campaigns have been launched to determine the effect of cloud radiative forcing on the Earth's atmosphere (*Arking,* 1991, *Chen et al,.* 2000). It is widely accepted that the clouds decrease the shortwave radiative flux at the surface by 40–50 Wm–2 , and they also decrease the outgoing longwave radiative flux by around 30 Wm–2 (*Ramanathan et al.,* 1989; *Wielicki et al.,* 1996; *Rossow* and *Duenas,* 2004). These effects result in a net diminution of 10–20 Wm–2 (*Chen* and *Rossow,* 2002; *Oreopoulos* and *Rossow,* 2011). However, the determination of the radiative forcing for each cloud and cloud type requires exact numerical models including accurate parameterization of cloud physical processes.

The necessity of a more detailed cloud radiation schemes in the modeling of cloud-radiation interactions has been permanently suggested during the last 30 years. It has been asserted by *Kunkel* (1984) and later by *Fouquart et al.* (1990) that a more accurate parameterization of cloud-radiation interactions is essential. *Buriez et al.* (1988) stated that until the '90s, optical characteristics had been tuned in the atmospheric models by arbitrary diagnostic cloud schemes to fit the results to the observations. *Harrington* (1997) showed that the applied parameterization technique in models strongly affects the optical properties of the simulated clouds. *Stephens* (2004) proved that the cloud properties such as optical depth, liquid and ice water contents, and particle size distribution significantly affect the radiation budget of Earth. Lack of correct data about optical properties of clouds is one of the major obstacles in determining the radiation budgets both of atmosphere and surface. According to *Stephens* (2004), the effect of clouds on heating and cooling of the atmosphere is a substantial feedback mechanism that had not been adequately investigated. Improvement in the numerical forecasting capacities of a weather forecasting model has been demonstrated in *Liu et al.* (2009). They have included detailed radiation scheme with microphysical size dependence in the U.S. Navy's Coupled Ocean-Atmosphere Mesoscale Prediction System (COAMPS) model. It has ultimately reduced the model's systematic warm bias, and overestimation of humidity in the upper troposphere. Comparing with measurements, the root mean square error of LW downward flux has changed from 17.67 Wm–2 to 9.44 Wm–2 in the case of standard model, and that of improved radiation model, respectively. *Petters et al.* (2012) highlighted that cloud radiative heating, and its feedback on cloud dynamics is largely sensitive to the number concentration of water droplets in stratiform clouds.

In numerical models, optical properties of warm clouds such as single scattering albedo and extinction coefficient are generally calculated by using a characteristic size of cloud droplets (*Lindner* and *Li*, 2000; *Ebert* and *Curry,* 1992). In these bulk schemes the size distribution of the droplets is generally given by an idealized gamma function with one or two independent parameters (*Ritter* and *Geleyn,* 1992; *Walko et al.*, 1995; *Straka et al.*, 2007; *Tompkins* and *Di Giuseppe,* 2009). The bulk models use the effective radius of cloud droplets and liquid water content to determine the optical properties (*Fu et al.,* 1998; *Hong et al.,* 2009, *Gettelman et al.,* 2008). Contrary to bulk schemes, bin microphysical schemes are capable to describe arbitrary size distribution of cloud droplets. In the case of bin schemes no assumption is needed on the droplet size distribution. While the bin schemes for the numerical simulation of cloud microphysical processes has been widely used since the early nineties, the application of this technique to calculate the optical properties of the clouds has become in the focus of researches in the last ten years. The advantage of the application of bin schemes for the calculation of cloud optical properties was proved by *Harrington* and *Olsson* (2001). They showed that the longwave radiation budget at the surface can be altered by 40 Wm^{-2} depending on how the effective radius of cloud droplets was calculated. The impact of using bin models on the cloud microphysical structure has been examined in *Harrington et al.* (2000). He has evaluated the effect of radiative cooling on the growth of water droplets. He showed that larger drops were growing faster than smaller drops. Drizzle-sized drops could be produced from 20 to 50 min earlier through the inclusion of the radiative term, which leads to a higher potential for enhancing drop collection and precipitation formation.

In this paper results about a new bin radiation scheme are presented. This technique was developed to calculate the extinction coefficients of water droplets in the infrared region. The impact of application of this new scheme on the longwave radiation budget is presented. The next section contains the description of the scheme. The results about the comparison with a bulk scheme are presented in Section 3. In Section 3.1, the changes in the extinction coefficients are presented. In Section 3.2, the change in the intensity of longwave radiation due to the application of bin scheme compared to the bulk scheme is studied. Section 3.3 examines the changes in the radiation profile with the help of the RRTM radiative transfer model, caused by the difference in the extinction coefficients. The conclusions are given in Section 4.

2. Description of the model

2.1. Description of the bin scheme

The optical parameters describing scattering, extinction, and absorption of radiation in clouds are: the extinction and scattering coefficients (β_{ext} and β_{sca});

the single scatter albedo (ω), which is the ratio of scattering in total extinction; and the asymmetry parameter (g), which characterizes the angle-dependence of the scattering (*Roach* and *Slingo,* 1979; *Stephens,* 1984; *Hu* and *Stamnes,* 1993). The definitions of these parameters for a given wavelength, in the case of water droplets assumed to be spherical are given in Eq. (1)−(4).

$$\beta_{ext} = \int_0^\infty A(D) Q_{ext}(D, m, \lambda) n(M) dM \quad , \tag{1}$$

$$\beta_{sca} = \int_0^\infty A(D) Q_{sca}(D, m, \lambda) n(M) dM \quad , \tag{2}$$

$$\omega = \frac{\beta_{sca}}{\beta_{ext}} \quad , \tag{3}$$

$$g = \frac{1}{2} \int_{-1}^1 p(\mu) \mu \, d\mu \quad , \tag{4}$$

where D is the droplet diameter, M is the mass of the droplet, λ is the wavelength, $n(M)$ is the droplet size distribution as a function of M, Q_{ext} is the extinction efficiency, Q_{sca} is the scattering efficiency, μ is the cosine of the scattering angle, and $p(\mu)$ is the phase function. m is the refraction index, $A(D)$ is the cross section.

The radiation transfer models and numerical models calculate the radiative transfer over radiation bands instead of calculating it at single wavelengths. For this purpose, a so-called broadband extinction coefficient is defined for an arbitrary wavelength interval of $\Delta\lambda$ (*Slingo* and *Schrecker* (1982)):

$$\beta_{ext} = \left(\int_{\Delta\lambda} E_\lambda \int_0^\infty A(D) Q_{ext}(D, m, \lambda) n(M) dM \, d\lambda \right) / \int_{\Delta\lambda} E_\lambda d\lambda \quad , \tag{5}$$

where E_λ is the Planck-function at a reference temperature (usually at 273 K). Bin scheme presented in details in *Rasmussen et al.,* (2002) is used to calculate the above integrals. The size range from 1.5625 μm to 5.07968 mm is divided into 36 bins with doubling the mass at the bin edges. The applied moment conserving technique allows us to describe the size distribution of water drops in every bin:

$$n_k(M) = A_k + M \cdot B_k. \tag{6}$$

.

The coefficients A_k and B_k are calculated from the number concentrations and mixing ratios in the kth bin (see more details in *Tzivion et al., 1987*). Using the bin scheme the Eq. (5) can be approximated by the following equation:

$$\beta_{ext} = \sum_{k=2}^{N_{bins}} [\int_{\Delta\lambda} (E_\lambda \int_{M_{k-1}}^{M_k} A(D)Q_{ext}(D,m,\lambda)n_k(M)dM\,d\lambda)/\int_{\Delta\lambda} E_\lambda\,d\lambda] \quad , \quad (7)$$

where N is the number of the bins, furthermore, M_{k-1} and M_k are the mass of the water drops at the edges of the kth bin.

The extinction coefficients can be calculated in every bin over any arbitrary wavelengths interval of $\Delta\lambda$. E_λ was calculated at $T=273$ K in this research. Sensitivity of the extinction coefficients on the temperature was investigated by calculating the above integral at $T_1=303$ K and $T_2=243$ K. Differences were found to be insignificant for the extinction coefficients for the whole infrared spectra. Comparing to the case of $T=273$ K, in the case of T_1 a little bit smaller value was calculated (the maximum difference was 0.17%), and in the case of T_2 a slightly larger value was calculated (maximum difference was 0.29%). Thus, the temperature dependence of extinction coefficients is neglected in this study.

The Q_{ext} extinction efficiency can be evaluated on the base of the Lorentz-Mie theory; however, it cannot be analytically calculated even in the case of spherical water drops. Instead of using time consuming numerical methods, the modified anomalous diffraction theory (MADT) was applied to describe the optical properties of water drops. *Mitchell* (2000) proved that application of this theory results in small errors comparing to the Lorentz-Mie theory. According to MADT, the extinction efficiency can be defined as a sum of two different components: the corrected Q_{ext}, and Q_{edge}:

$$Q_{ext,m}(D,\lambda,m) = (1+\frac{C_{res}}{2})Q_{ext} + Q_{edge} \quad . \quad (8)$$

The details about calculation of C_{res}, Q_{ext}, and Q_{edge} variables can be found in Appendix A.

As the $Q_{ext}(D,\lambda,m)$ function has been given in explicit form, the integrals in Eq. (7) can be calculated by taking into consideration the $n_k(M)$ size distribution given by Eq. (6). The evaluation of the integrals in Eq. (7) can be made to be very fast, if two two-dimensional kernels were precalculated over the two-dimensional grid defined by both mass intervals and wavelength intervals of the radiative transfer model described in Section 2.3.

The details about the calculation of $K_{Akj}(M_{k-1},M_k,\Delta\lambda_j)$ and $K_{Bkj}(M_{k-1},M_k,\Delta\lambda_j)$ are given in Appendix B. These coefficients can be implemented in the radiative transfer model afterwards, to yield extinction coefficients for the new bin method.

2.2. Description of the bulk scheme

Because the computational cost of the bin scheme is high, it is important to investigate whether the optical parameters defined by the Eqs. (1) – (4) are sensitive on the method they are calculated. In this study, extinction coefficients (Eq. (1)) obtained by bin scheme are compared to the extinction coefficients obtained by a bulk scheme method (*Hu* and *Stamnes,* 1993). This parameterization is currently used to calculate extinction coefficients in the RRTM LW radiation transfer model. More details about this model are given in Section 2.3.

The method developed by *Hu* and *Stamnes* (1993) is a frequently applied bulk parameterization scheme, which uses the effective radius and the liquid water content (*LWC*) as input parameters:

$$\beta_{ext} / LWC = a\, r_e^b + c .$$

(9)

The *a, b, c* coefficients are defined for the following three intervals of the effective radius: $2.5 - 12$ μm; $12 - 30$ μm; and $30 - 60$ μm, and for 50 wavelength bands in the infrared spectrum. This scheme is based on Mie-scattering calculations, which is appropriate method to determine the $Q_{ext}\,(D,m,\lambda)$ extinction efficiency, at any wavelengths and droplet diameters. The *n(M)* droplet size distribution was assumed to be a gamma-size distribution:

$$n^{*}(r) = \frac{N_0}{\Gamma(\gamma)\, r_m} \left(\frac{r}{r_m}\right)^{\gamma - 1} \exp^{-r/r_m} ,$$

(10)

where N_0 is the total (volume) number concentration, Γ is the gamma function, r_m is the characteristic radius of the size distribution, and γ is a constant, that defines the shape of the distribution (*Stephens et al.*, 1990).

The *a, b, c* coefficients were calculated by least-square fitting of Eq. (9) on the set of extinction coefficients related to data pairs of effective radius and liquid water content. The effective radii and liquid water content were calculated by using different shape parameters (γ), characteristic sizes (r_m), and total number concentrations (N_0) in Eq. (10). This group of data was set up for 50 predefined wavelengths, ranging from 3.9 μm to 150 μm (*Hu* and *Stamnes,* 1993).

2.3. Description of the radiative transfer model

The RRTMG LW (rapid radiative transfer model for the longwave radiation) (*Clough et al.*, 2005) radiation model is used in our studies to calculate the longwave fluxes in the case of different clouds. It has been developed for the

calculation of longwave atmospheric fluxes and cooling rates in atmospheric radiative transfer studies, as well as for implementation in numerical weather prediction and climate models.

The longwave spectrum is divided into 16 bands in the RRTM, from 3.33 μm to 1000 μm, according to the main absorption bands of the atmospheric gases at different wavelengths (*Table 1*). These bands have been determined to have maximum two main absorbing compounds in each band; to limit the variation of the Planck function within the bands; and to keep the number of bands minimized as possible while keeping the previous two conditions. The model is capable to take into account the radiative effects of water vapor, carbon dioxide, ozone, nitrous oxide, methane, oxygen, nitrogen, and halocarbons. The two main compounds (water vapor, carbon dioxide) were taken into consideration in present calculations.

Table 1. Wavelengths intervals of the RRTM model

Band	Wavelength (μm)	1050–96 (hPa)	96–0.01 (hPa)
16	40.00 – 1000.00	H_2O	H_2O
15	20.00 – 40.00	H_2O	H_2O
14	15.90 – 20.00	H_2O, CO_2	H_2O, CO_2
13	14.30 – 15.90	H_2O, CO_2	CO_2, O_3
12	12.20 – 14.30	H_2O, CO_2	CO_2, O_3
11	10.20 – 12.20	H_2O	–
10	9.26 – 10.20	H_2O, O_3	O_3
9	8.47 – 9.26	H_2O	O_3
8	7.19 – 8.47	H_2O, CH_4	CH_4
7	6.76 – 7.19	H_2O	H_2O
6	5.55 – 6.76	H_2O	H_2O
5	4.81 – 5.55	H_2O, CO_2	–
4	4.44 – 4.81	H_2O, N_2O	–
3	4.20 – 4.44	CO_2	CO_2
2	3.85 – 4.20	N_2O, CO_2	–
1	3.33 – 3.85	H_2O, CH_4	–

The development of RRTM has been based on the calculations made by the line-by-line radiative transfer model (LBLRTM) (*Mlawer et al*., 1997). The absorption coefficients for different temperatures, pressures, and relative amount of the absorption gases have been determined by this model. These constants are imported as look-up-tables into the RRTM model, and linear interpolation is used to calculate the absorption coefficients at the actual temperature, pressure, and gas concentration.

The radiative transfer is calculated in the RRTM model for all of the 16 spectral bands, as if it was a single spectral wavelength. In the case of vertically inhomogeneous layers, it uses the Pade's approximation to calculate effective Planck function for each layer, by using the temperatures at boundaries of layers, and mean layer temperatures (*Clough et al., 1992; Mlawer et al., 1995*). The variation of the Planck function in a band according to the wavelength is taken into account by weighting according to the abundance of main gas compounds related to the band. (*Mlawer et al.,* 1995).

In RRTM the correlated-k method is used to describe the wavelength-dependency of the absorption coefficients in the radiative transfer equations. The correlated k-technique is an approximation method with high accuracy. It is frequently applied for the calculation of radiative transfer radiances by transforming the integral over wavelength into integral over a cumulative probabilistic function. This function is determined by rearranging the absorption coefficient values in ascending order according to the fraction of the given value in the actual wavelength band (*Mlawer et al.,* 1997). This generates a new order of the absorption coefficients according to their probability. A characteristic average value of the absorption coefficient in a given probability-interval is then defined, and used in the radiative transfer equations to calculate the radiances.

The values of the probability function at given pressure and temperature are calculated beforehand by a line-by-line radiative transfer model. In the RRTM, they are interpolated linearly between the logarithm of temperature and pressure values. Also, linear weighting of the absorption coefficients is done according to their integrated line strengths and column amount, when two different species are dominant in the same spectral band. These simplifications make this method computationally fast, meanwhile keeping the needed accuracy.

Validation of the RRTM model shows that RRTM results agree with those computed by the line-by-line model within $1.0\,\mathrm{Wm}^{-2}$ at all levels, and the computed cooling rates agree to within 0.1 K/day in the troposphere and 0.3 K/day in the stratosphere (*Clough et al.,* 2005). The RRTM model has been implemented as the operational code for longwave radiation at the European Center for Medium-Range Weather Forecasts (ECMWF) and in the Global Forecast System (GFS) of the National Centers for Environmental Prediction (NCEP). It is also implemented as one option in the National Center for Atmospheric Research (NCAR) Weather Research and Forecasting (WRF) model.

3. Results

3.1. Comparison of the extinction coefficients calculated by bin and bulk schemes

Extinction coefficients calculated by bin and bulk schemes are compared in this section. The investigated cases are described in *Table 2*. The first column gives

the number concentration, the second, third, and fourth ones show the effective radii if $LWC_1 = 10^{-3}$ kg m^{-3}, $LWC_2 = 10^{-4}$ kg m^{-3}, and $LWC_3 = 10^{-5}$ kg m^{-3}, respectively. The size distributions of the water drops were given by Eq. (10), and the value of γ parameter was chosen to be equal to 3.

Table 2. Effective radius for gamma-distributions for different number of concentration and LWC values

	$LWC_1 = 10^{-3}$ kg m^{-3}	$LWC_2 = 10^{-4}$ kg m^{-3}	$LWC_3 = 10^{-5}$ kg m^{-3}
N_i (*10^6) 1/m^3	r_{eff} (*10^{-6}) m	r_{eff} (*10^{-6}) m	r_{eff} (*10^{-6}) m
1000	7.92	3.68	–
250	12.57	5.84	2.71
100	17.07	7.92	3.67
50	21.50	9.98	4.63
20	29.18	13.55	6.29

It has been found that the changes in the difference between the extinction coefficients calculated by the bin and by the bulk scheme depends mostly on the value of the effective radius of the size distribution, regardless of the values of the LWC and the number concentration of water droplet. E.g., the differences between the bin scheme and the bulk scheme were very similar in the following two cases: $LWC_2 = 10^{-4}$ kg m^{-3}, N = 1000·10^6 m^{-3} and $LWC_3 = 10^{-5}$ kg m^{-3}, N = 100·10^6 m^{-3}.

Fig. 1 summarizes the results obtained at $LWC_1 = 10^{-3}$ kg m^{-3} at two different concentrations of the droplets, and *Fig. 2* summarizes the results obtained at $LWC_2 = 10^{-4}$ kg m^{-3}, at two different number concentrations.

Fig. 1 and *Fig. 2* show that the difference between the extinction coefficients depends both on the wavelength and on the effective radius. Because the surface and the atmosphere emit most of the energy in the wavelength interval of 5−20 μm, the difference between the results of the schemes will be analyzed in this interval. The relative difference can be higher than 20% if the effective radius is lower than 10 μm. There is no significant (maximum 4%) difference between the calculated extinction coefficients if the effective radius is higher than about 10 μm, and the wavelength is less than about 8.0 μm. Although the local minimum values at near to the wavelength of 10 μm given by the different schemes are very similar, the application of the bulk scheme results in much sharper decrease and increase of the extinction coefficients in the wavelength interval of 10−15 μm.
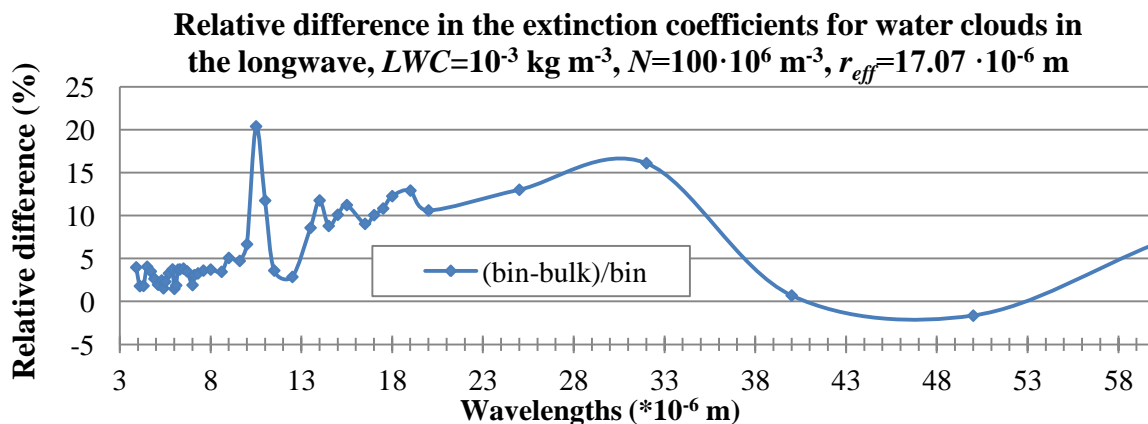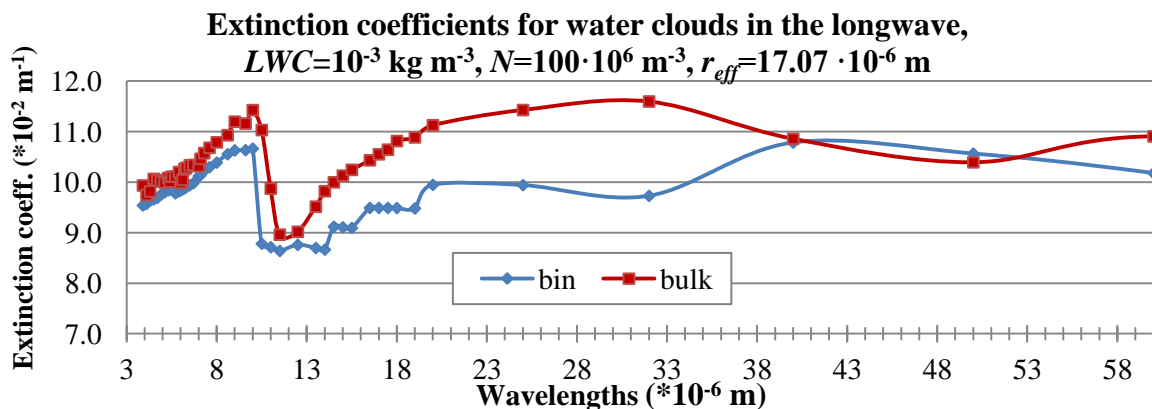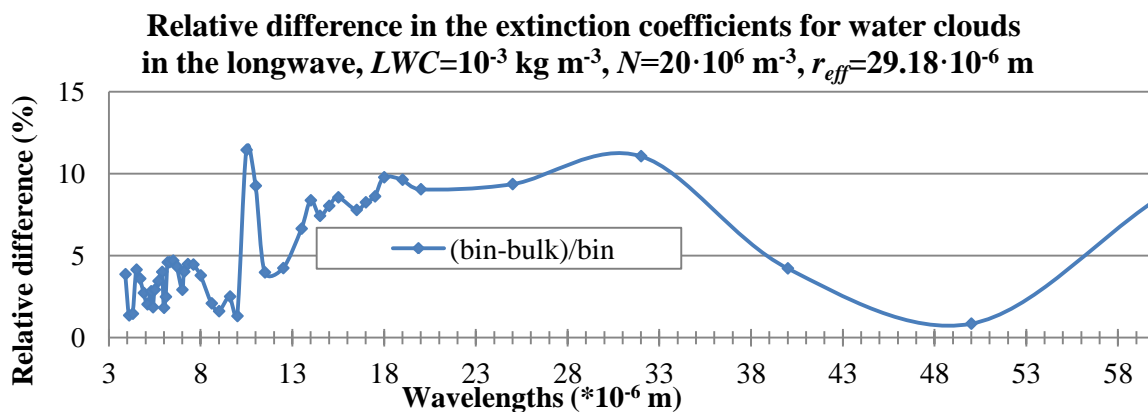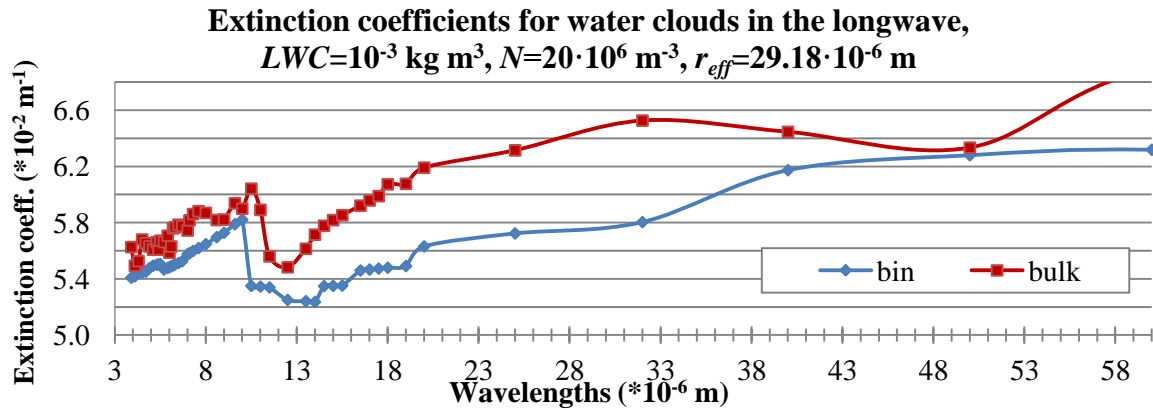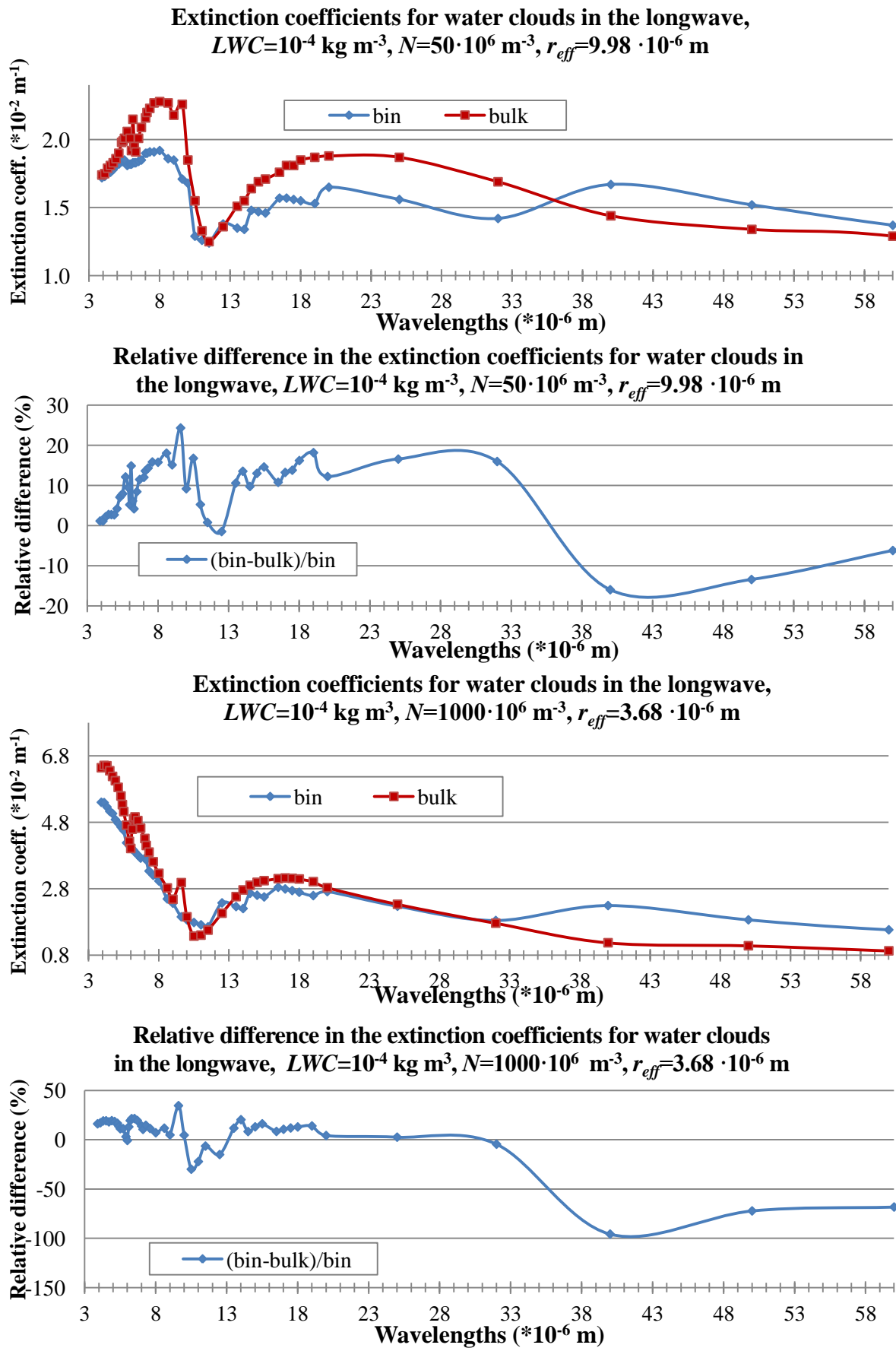
Fig. 1. Extinction coefficients and relative differences calculated for two different gamma-size distributions (N=20, and $100·10^6$ m^{-3}, LWC=10^{-4} kg m^{-3}).

Extinction coefficients for water clouds in the longwave, $LWC=10^{-4}$ kg m^{-3}, $N=50 \cdot 10^6$ m^{-3}, $r_{eff}=9.98 \cdot 10^{-6}$ m

Relative difference in the extinction coefficients for water clouds in the longwave, $LWC=10^{-4}$ kg m^{-3}, $N=50 \cdot 10^6$ m^{-3}, $r_{eff}=9.98 \cdot 10^{-6}$ m

Extinction coefficients for water clouds in the longwave, $LWC=10^{-4}$ kg m^3, $N=1000 \cdot 10^6$ m^{-3}, $r_{eff}=3.68 \cdot 10^{-6}$ m

Relative difference in the extinction coefficients for water clouds in the longwave, $LWC=10^{-4}$ kg m^3, $N=1000 \cdot 10^6$ m^{-3}, $r_{eff}=3.68 \cdot 10^{-6}$ m

Fig. 2. Extinction coefficients and relative differences calculated for two different gamma-size distributions ($N=50$, and 1000 10^6 m^{-3}, $LWC=10^{-4}$ kg m^{-3}).

In the critical wavelength interval near to the wavelength of 10 μm – where the absorption of both vapor and CO_2 is relatively small and the absorption of the water drops can be dominant –, significant difference can be found between the results of bulk and that of bin scheme if the effective radius is between 3–15 μm. In this size range, significant positive difference (larger than 10%) can be observed in the whole spectra, except at a narrow wavelength interval of 10–13 μm, where at 9.6 μm wavelength, the difference is much higher for all effective radius values. In case of larger effective radius (>10 μm), the difference is getting smaller, and is getting more emphasized above the wavelength of 10 μm.

It has to be noted that the comparison was made by using idealized gamma size distribution in the case of bin scheme as well. In the real clouds the size distribution of the water drops can significantly differ from the gamma size distribution. The difference between the two schemes shows that the application of effective radius and the liquid water for evaluating the optical properties may results in overestimation of the extinction coefficient mostly in the case of relatively high concentration of the larger water droplets..

It can be established that the bin scheme gives generally smaller value than the bulk scheme does, except at large wavelengths (λ>33 μm), and except at wavelength interval of 10–13 μm in the cases of smaller effective radii. If r_{eff}>20μm, the bulk scheme gives always higher value than the bin scheme does.

From *Figs. 1* and *2*, it can be concluded that the curves related to the extinction coefficients calculated by the bin scheme are smoother; they do not fluctuate by the wavelength as sharply as it can be observed in case of a bulk scheme. The reason for this is that bulk scheme uses only the r_{eff} drop size, and radius much different from this characteristic size are not represented in calculation; whereas the bin scheme allows us to take into account the extinction caused by any drop sizes.

3.2. *Comparison of the longwave outgoing radiations at top of cloud layer*

In this section results about the longwave outgoing radiation at the top of a cloud layer are presented. The calculations were made for 100 m deep cloud layers with different liquid water contents and drop concentrations. To focus on the effect of water drops, the absorption of the vapor and that of CO_2 was not taken into consideration in the radiative transfer model in this section. It was assumed that the cloud base temperature is 293 K and the vertical temperature gradient is wet adiabatic. The emitted thermal radiation goes through the 100 m thick cloud characterized by different microphysical parameters. The number concentration and *LWC* values of these clouds are given in *Table 1*. The cases presented in *Figs. 3* and *4* are the same cases as in *Figs. 1* and *2*.

The RRTM model described in Section 2.3 was used for calculating the radiation transfer. The new bin scheme has been implemented into the RRTM

model. The two dimensional arrays of K_{Akj} ($M_{k-1}, M_k, \Delta\lambda_j$) and K_{Bkj} ($M_{k-1}, M_k, \Delta\lambda_j$) were precalculated, and were used during the simulations.

This development is a novel one, as the RRTM model has been capable to use only the bulk scheme described in Section 2.2. In the case of bulk scheme, the input parameters for the cloud profiles are the effective radius and the cloud water path (which is the LWC multiplied by cloud thickness). Now RRTM can be coupled to a detailed microphysical model, which gives the thickness of the cloud layer, and A_k and B_k coefficients (defined in Section 2.1) for each bin as input data.

The results are summarized in *Table 3*. The first column gives the number concentrations, the second, third, and fourth ones give the difference between the intensities calculated by bin and bulk schemes at different liquid water contents.

Table 3. Difference of the radiation intensity (bin-bulk) at different number of concentration and *LWC* in the case of 100-m-thick cloudy layer, water vapor and CO_2 is not included

N_i (*E+06) 1/m³	LWC_1=10^{-3} kg m⁻³ r_{eff} (*10^{-6}) m	LWC_2= 10^{-4} kg m⁻³ r_{eff} (*10^{-6}) m	LWC_3= 10^{-5} kg m⁻³ r_{eff} (*10^{-6}) m
1000	10.70	10.28	–
250	11.35	10.83	–
100	11.77	11.18	4.37
50	12.07	11.35	4.17

The data in *Table 3* show that the application of bin scheme results in about 11 Wm–2 larger outgoing energy in a second at the top of a 100-m-thick cloud when the amount of liquid water content is about 10^{-4} kg m⁻³, and no significant increase between the differences can be observed if the liquid water content was increased by one order. In the case of $LWC_3 = 10^{-5}$ kg m⁻³, the difference is about a factor of 2. This decrease of difference between the outgoing radiations corresponds with results of pervious Section. This shows that although the relative difference between the extinction coefficients calculated by different schemes depends mostly on the effective radius, the difference between the calculated intensities of radiation depends on the absolute value of the extinction coefficient, which is higher in the case of higher LWC values. It also stems from data in *Table 3* that the extinction becomes saturated in the clouds with increasing *LWC*. This is the reason why there is no further significant change in the difference of the calculated intensities as the liquid water content increases from 10^{-4} kg m⁻³ to 10^{-3} kg m⁻³.

The differences between the two schemes at the cloud top in each band have been plotted in *Figs. 3* and *4* for the four cases presented in *Figs. 1* and *2*. It can be seen that the majority of the differences appears in the bands of 1–12, which corresponds with the wavelengths interval of 3.3–14.3 μm. It means that the main difference comes from this wavelengths band, as already stated in Section 3.1. The highest difference for all cases is in band 6. The peak of the Planck function at T=293 K is at 9.88 μm (band 10 of RRTM), so the wavelengths band with the maximum change between the two schemes is not correlated with the maximum of the Planck function. It can be due to the different methods that the bulk scheme and the bin scheme uses for calculating averaged extinction coefficients for the wavelengths bands.
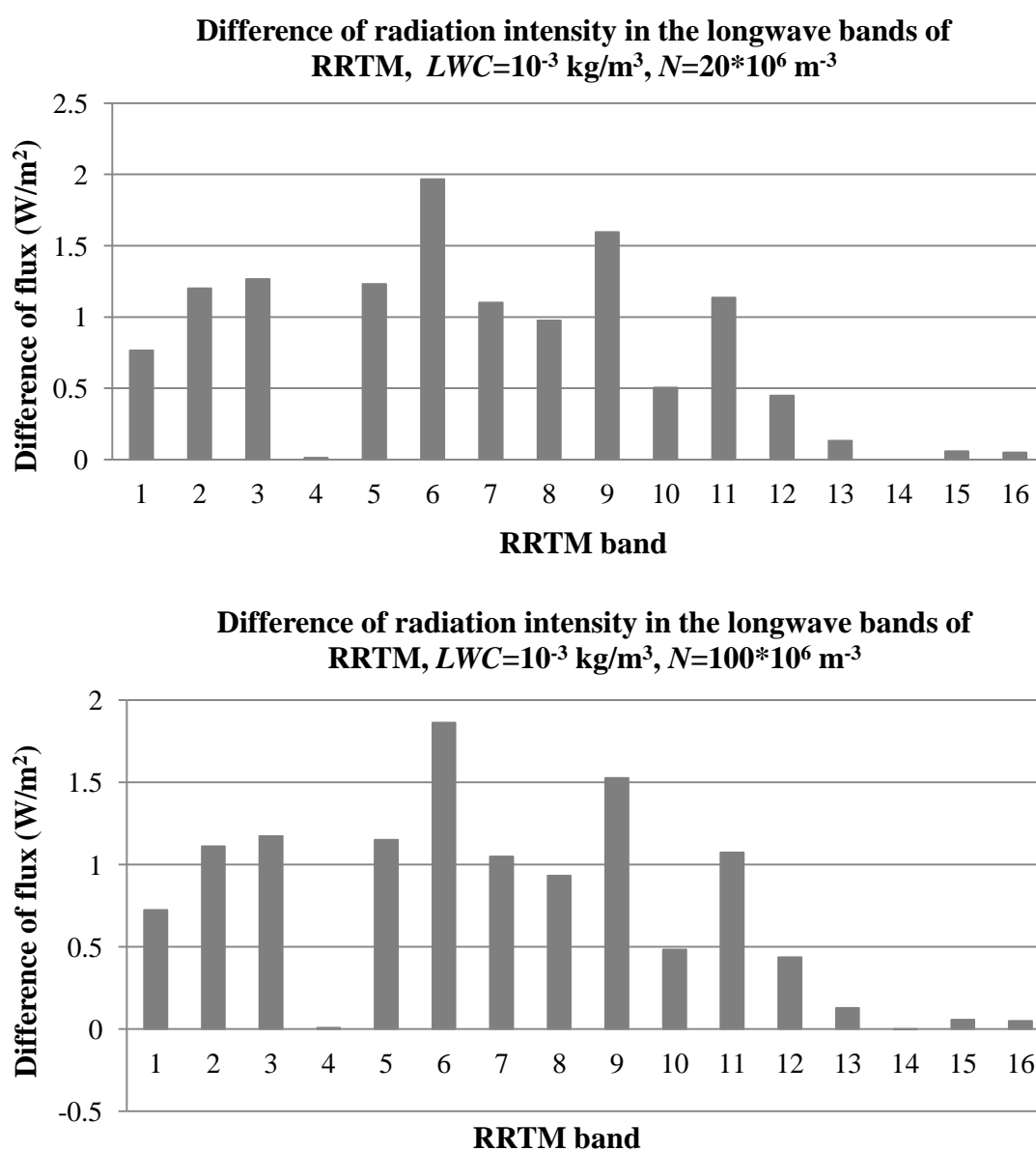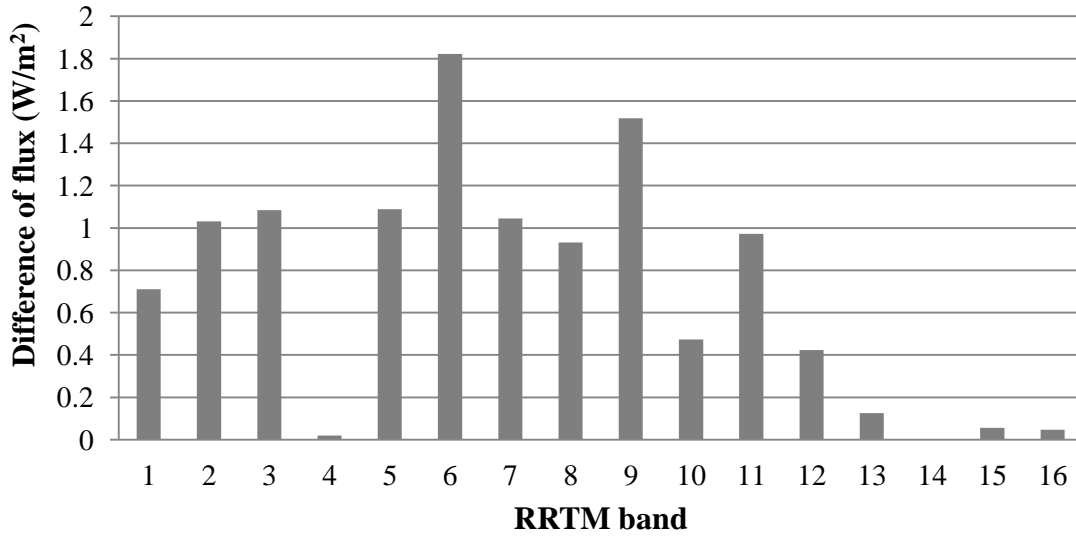
Difference of radiation intensity in the longwave bands of RRTM, $LWC=10^{-3}$ kg/m^3, $N=20*10^6$ m^{-3}

Difference of radiation intensity in the longwave bands of RRTM, $LWC=10^{-3}$ kg/m^3, $N=100*10^6$ m^{-3}
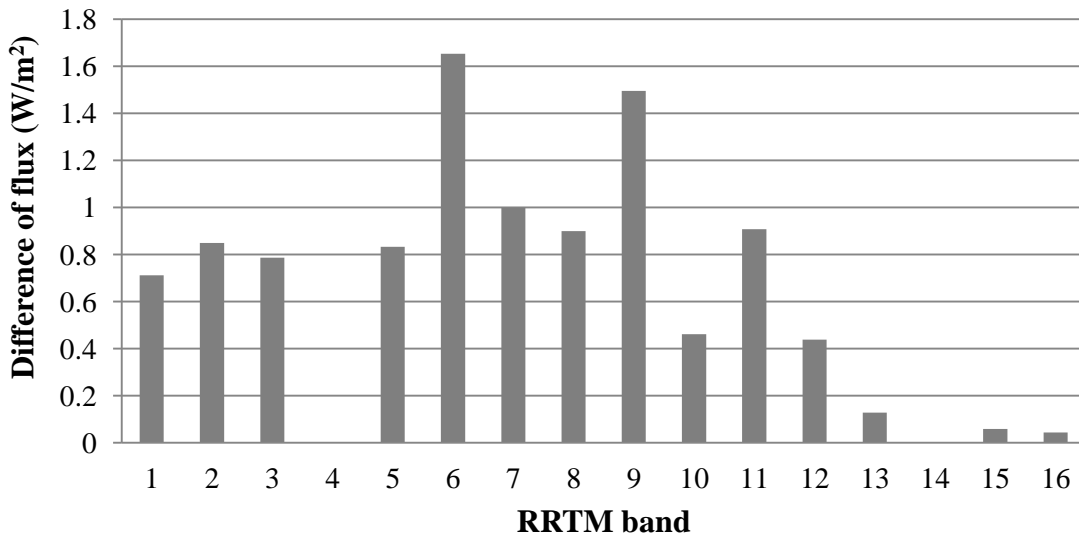

Fig. 3. Differences between the two schemes (bin-bulk) at different bands. $LWC=10^{-3}$ kg m^{-3}, the values of *N* are given at the top of the figures.

Difference of radiation intensity in the longwave bands of RRTM, $LWC=10^{-4}$ kg/m^3, $N=50*10^6$ m^{-3}

Difference of radiation intensity in the longwave bands of RRTM, $LWC=10^{-4}$ kg/m^3, $N=1000*10^6$ m^{-3}

Fig. 4. Differences between the two schemes (bin-bulk) at different bands. $LWC=10^{-4}$ kg/m^3, the values of N are given at the top of the figures.

Control calculations show that presence of vapor and CO_2 reduces the difference between the schemes by a factor of two. The largest difference was found to be 6.11 W m^{-2} at $N = 20 \cdot$m^{-3} and $LWC = 10^{-3}$ kg m^{-3}. In the presence of vapor and CO_2, no significant difference is shown in channels 1–4, difference is significant in channels 5–9 where the Planck energy is relatively high.

3.3.   Results of the application of bin scheme in RRTM model

In this section the results about the upward and downward radiation profiles are presented. The atmospheric radiation profiles with the RRTM model for four different clouds were calculated. The thickness of the clouds, the number concentration of cloud droplets, and the liquid water content in the clouds are summarized in *Table 4*. In the case of fog the base was at the surface, and *LWC* was constant. In the case of the cloud the cloud base was at 400 m, and the *LWC* linearly increased until 625 m (where $LWC=5 \cdot 10^{-4}$kg m^{-3}), and above this height it linearly decreased. The size distribution of the water drops was given by Eq. (10) in both schemes.

Table 4. The summary of the investigated cases. * indicates mean value in the cloud layer.

Abbr.	Thickness (m)	N (*10^6 1/m^3)	LWC (10^{-3} kg m^{-3})
fog50	100	50	1
fog100	100	100	1
cloud100	300	100	2.5
cloud500	300	500	2.5

The water vapor and temperature profiles used for the calculation are plotted in *Figs. 5 and 6*. The temperature gradient was 0.976 K/m below the cloud, and it was 0.7 K/m above the fog and the cloud, and the temperature was constant above 12 km. In the cloud wet adiabatic temperature profile was supposed. The water vapor mixing ratio was equal to the saturation values within the clouds, and it decreased linearly above the cloud (and the fog) top until the height of 9 km, where it became equal to zero.
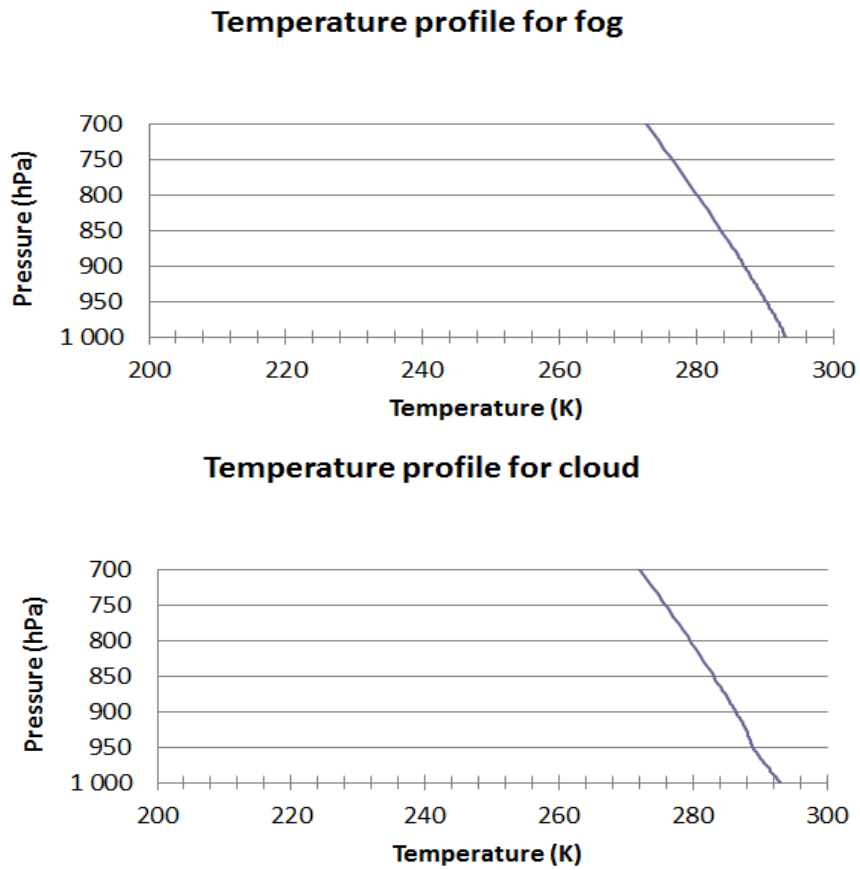
Temperature profile for fog

Temperature profile for cloud

Fig. 5. Temperature profiles for the cloud and fog cases.

Water vapour profile for fog
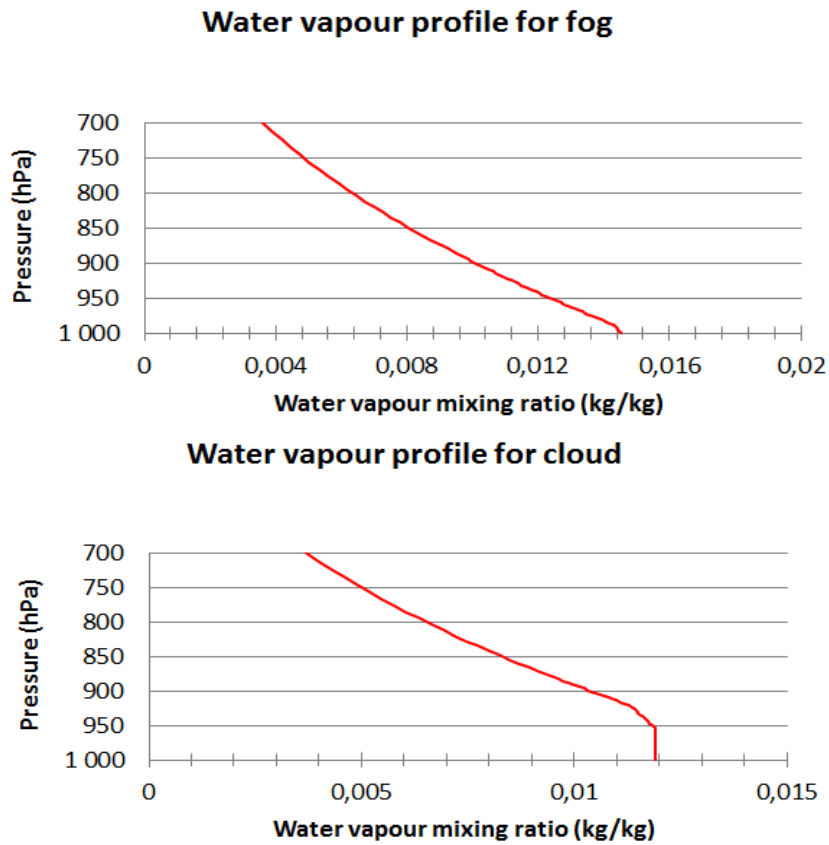

Water vapour profile for cloud

Fig. 6. Water vapor profiles for the cloud and fog cases.

The results of the RRTM calculations are shown in *Figs. 7–10*. While the upward radiation profiles were hardly affected by modification of scheme, the downward profiles were more significantly sensitive on the applied scheme. In the case of the fog, the difference between the intensity of the downward radiations at the surface is about 20 Wm^{-2}. In the case of the cloud, similar difference can be observed at about 100 m below of the cloud top. More absorption is observed in the case of the bin scheme (when absorption is closer to 1, the net flux is closer to 0). Comparison of fog50 and fog100 cases shows that the difference between the two schemes is hardly affected by the number concentration of the water droplets.
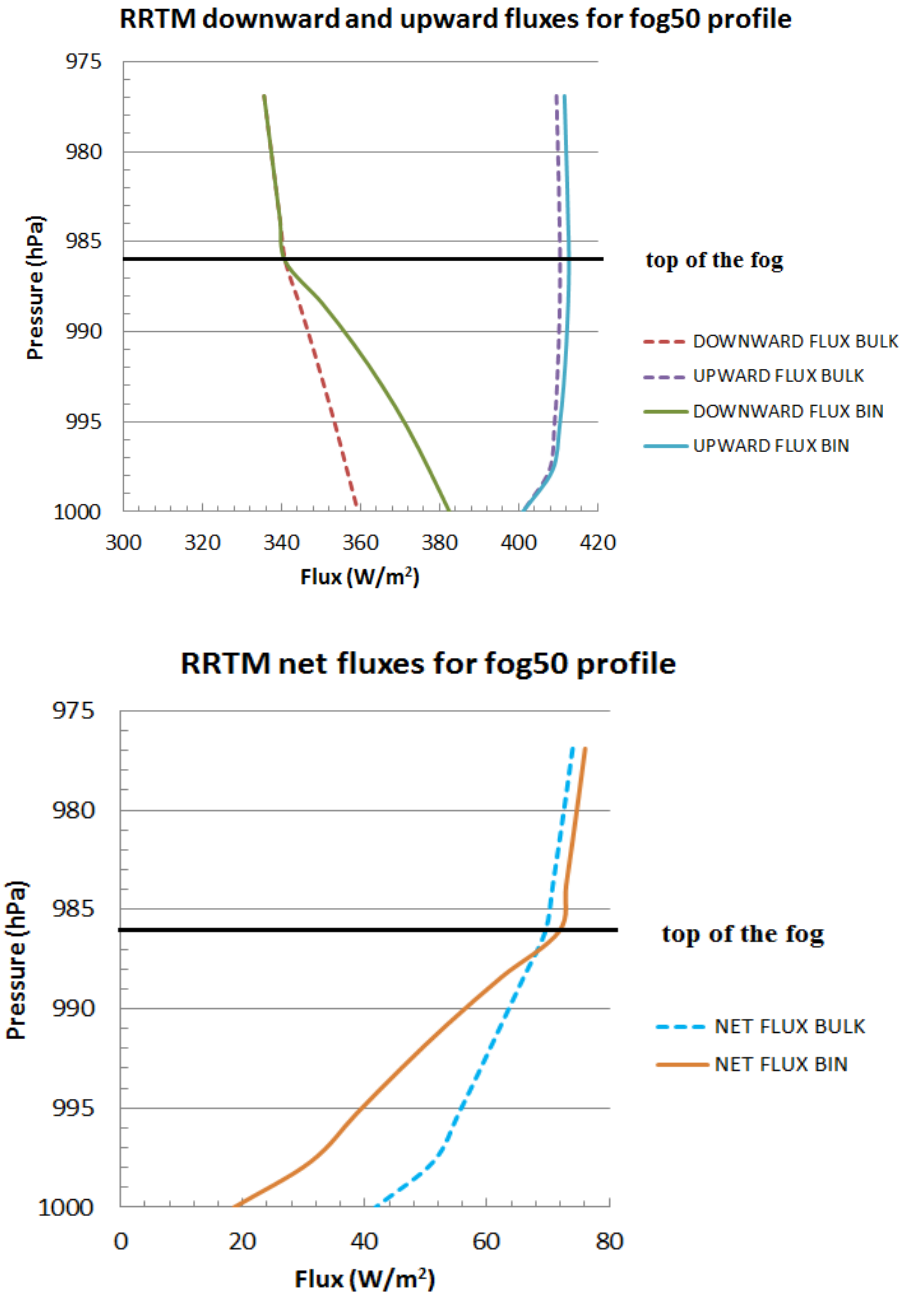

Fig. 7. Upward, downward, and net radiation flux profiles in fog50.

RRTM downward and upward fluxes for fog100 profile
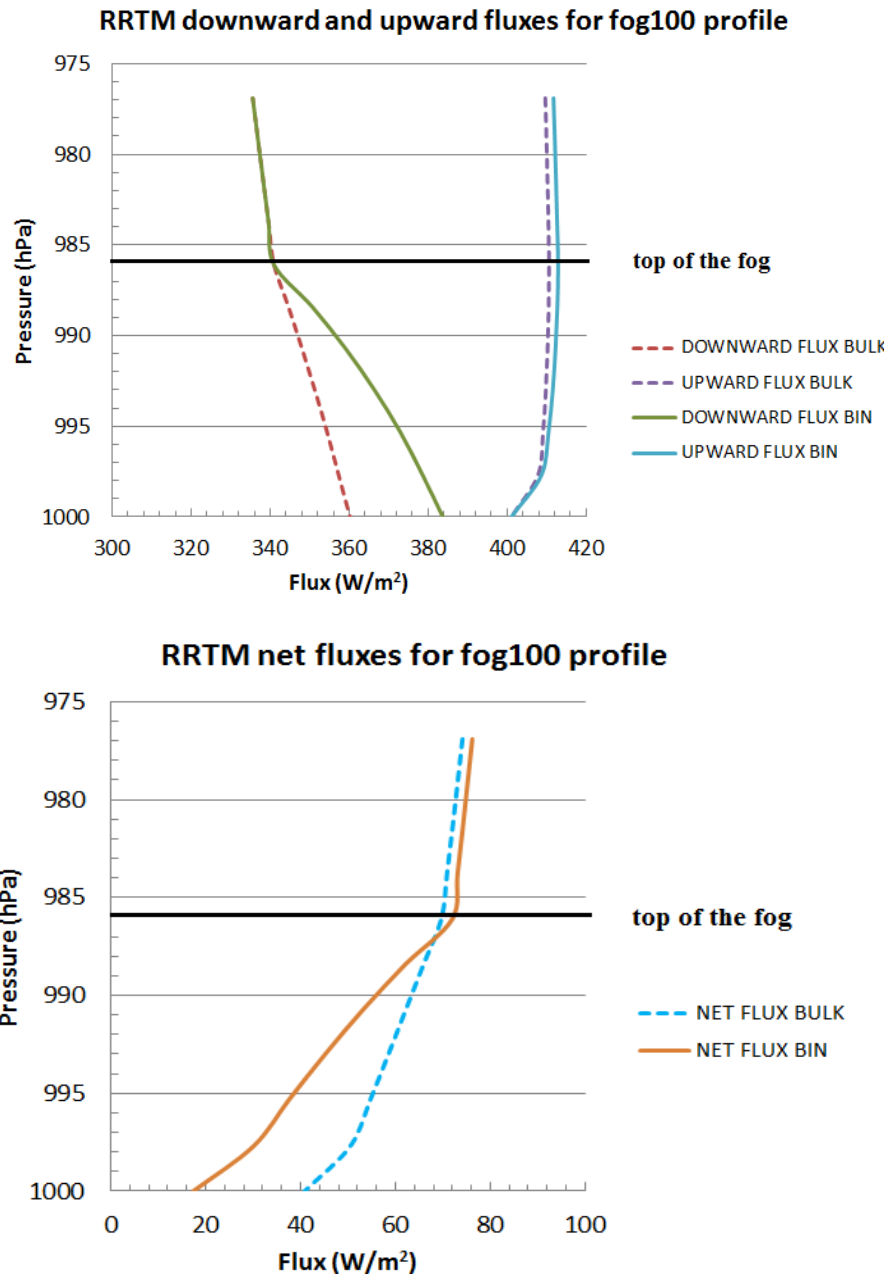
RRTM net fluxes for fog100 profile

Fig. 8. Upward, downward, and net radiation flux profiles in fog100.

It can be also noted in *Figs. 9* and *10* that the absorption of the downward radiation is more intense in case of the bin scheme than in the bulk scheme. In the cloud layer the net radiation (the difference between the downward and upward radiation) is close to zero in the case of the bin scheme and slightly larger than zero in the case of bulk scheme. This means that the absorption within the cloud is almost 1. Considering the net fluxes, the maximum difference between the two profiles is around 30 Wm^{-2} in case of clouds and 20 Wm^{-2} in the case of the fog. As the gradient of the net flux is different within the cloud layer, the heating/cooling rate is larger in case of the bin scheme, because the flux is changing more sharply. Thus, difference between the schemes can impact both the cloud dynamics and cloud microphysics.

The different schemes give significantly different gradients of the net radiation in both cloud100 and cloud500 cases. The difference between the schemes is more significant in the case of cloud500, both at the cloud base and at the cloud top. So it can be concluded that the number of concentration of the droplets affect the gradient of the net fluxes, and subsequently the cooling rate at the cloud edges. The maximum cooling rate at the top of the layer in case of fog50 was 34.5 K/day in the bin scheme; whereas in the bulk scheme, it was only 12.9 K/day.

It can be seen from *Figs. 9* and *10* that if the cloud layer is thinner (100 m in case of the fog), the difference in the net outgoing radiation between the two schemes is much higher than in case of the 300-m-thick cloud.
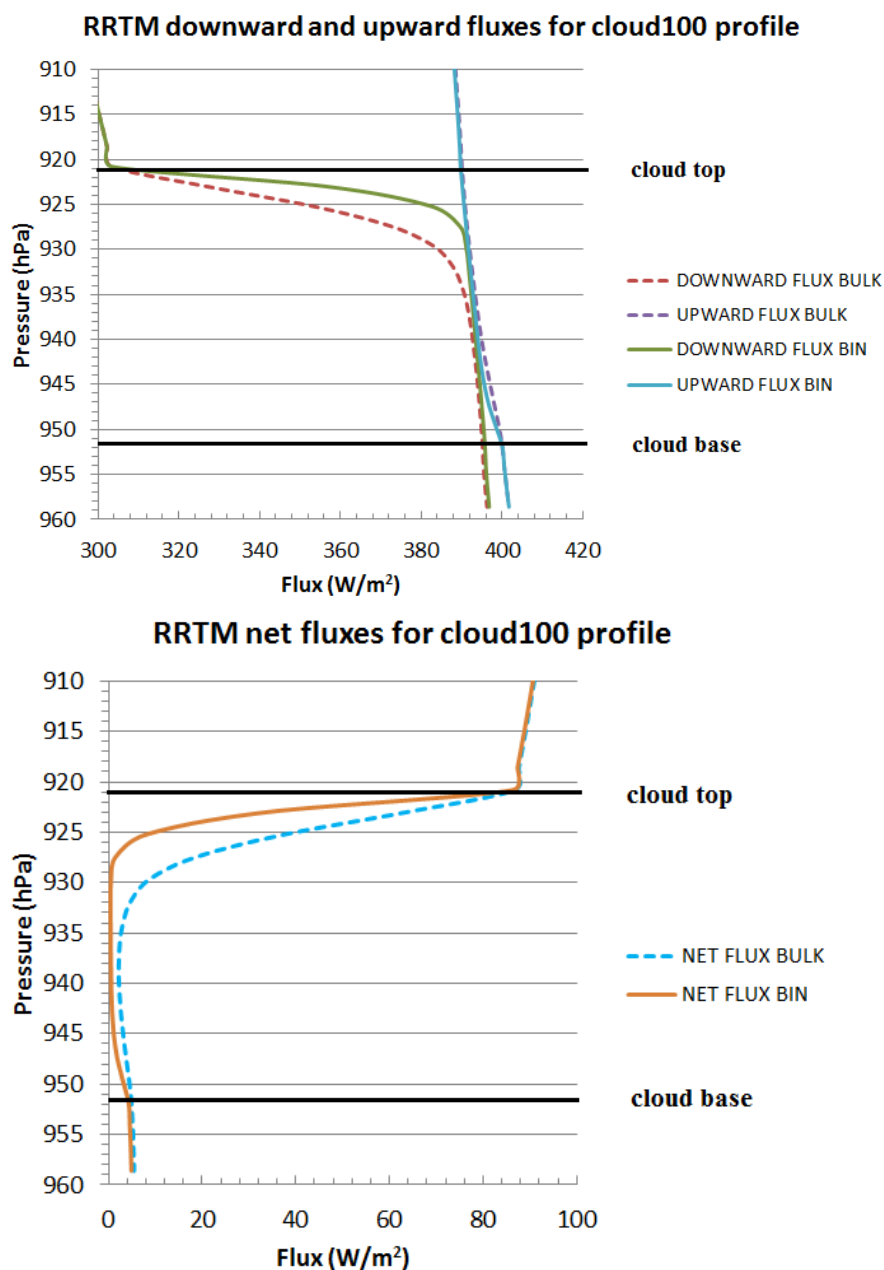

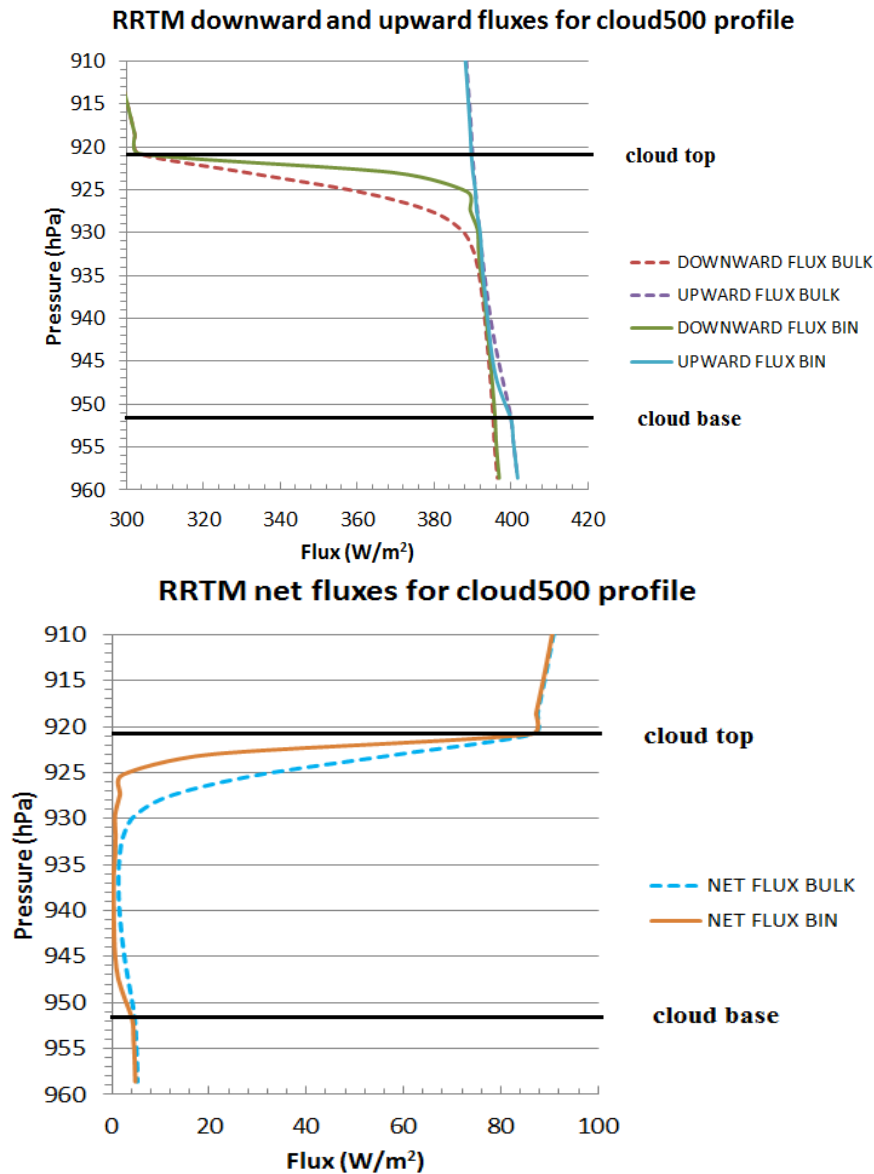*Fig. 9.* Upward, downward, and net radiation flux profiles in cloud100.

Fig. 10. Upward, downward, and net radiation flux profiles in cloud500.

4. Conclusion

Cloud-radiation interactions are essential to be understood and modeled correctly. The evolving radiation profile affects temperature and microphysical processes in micro-scale, and atmospheric motions in larger scales. Weather events and climatic patterns strongly depend on the radiation budget. More accurate description of cloud optical properties can significantly improve numerical weather forecasts.

In this study it was investigated how evaluation of the extinction coefficients affects longwave radiation budget, and longwave heating/cooling rates in the atmosphere. A new bin radiation scheme was developed, and the results of bin scheme were compared to that of a currently applied bulk scheme, which is widely used in operational numerical weather prediction models.

The results are summarized in the following points:

(1) The extinction coefficient calculated by the bin scheme was generally smaller than that calculated by the bulk scheme. The difference between the extinction coefficients calculated by the two different ways depends on the effective radius and the wavelength. The two curves fit well in the whole spectrum if the effective radius is higher than 10 μm, and the wavelength is less than about 8.0 μm. In the case of the smaller effective radius, or higher wavelengths, significant difference was found in the wavelength interval of 5–20 μm (around 10%), and even higher at the wavelengths of 9.6 μm for all effective radii.

(2) The variations of the extinction coefficients in the bin scheme are smoother than in the bulk scheme, due to the fact that the bin scheme represents a broad size of droplet spectra, compared to the bulk scheme which is represented by a single effective radius.

(3) The two different methods for the calculation of the extinction coefficients result in an increase of about 10 Wm^{-2} in the outgoing longwave radiation in case of a 100-m-thick cloud layer when the effect of the water vapor and CO_2 is not taken into account. The change in the intensity was two times smaller if the *LWC* was reduced to 10^{-5}kg m^{-3} within the cloud. The main difference comes from the wavelengths bands below 14 μm, where the majority of the Planck energy is. The presence of the vapor reduces the difference between the two schemes.

(4) The number of concentration in the cloudy layer does not affect considerably the resulting difference between the outgoing radiations calculated by the two schemes. However, the value of *LWC* and the cloud thickness have larger impact: the lower the *LWC*, and the higher the cloud thickness is, the smaller the difference between the two schemes.

(5) Large uncertainty of net radiation at surface can result in significant error in the forecast of the surface temperature. Supposing steady state conditions, the difference of 20 Wm^{-2} can results in about 3 C differences in surface temperature after 6 hours.

(6) Large difference (30 Wm^{-2}) between the two schemes was found within the simulated cloud layer near to the cloud tops. 20 Wm^{-2} difference between the net longwave radiations was found at the surface in case of fog.

(7) The bin scheme produced profiles with higher gradient at the edges of the cloud layer, which results in higher cooling rate as well both at the cloud top and cloud base. In the case of the bulk scheme, temperature hardly changes at the cloud base, which results in negligible warming. The consequence of different temperature profiles given by the two schemes can be significantly different cloud microphysics and cloud dynamics.

At the next phase of the research, the RRTM model will be coupled with a two-dimensional cloud model. The model uses bin microphysics, which allows us to give an appropriate input for the recently developed bin radiation scheme.

References

Arking, A., 1991: The Radiative Effects of Clouds and their Impact on Climate. *B. Am. Meteorol. Soc*. *72*, 795–953.

Buriez, J.C., Bonnel, B., Fouquart, Y., Geleyn, J.F., and *Morcrette, J.J.,* 1988: Comparison of model-generated and satellite- derived cloud cover and radiation budget. *J. Geophys. Res. 93*, 3705–3719.

Chen, T., Rossow, and *W.B., Zhang, Y.*, 2000: Radiative Effects of Cloud-Type Variations. *J. Climate*, *13*, 264–286.

Chen, T., and *Rossow*, *W.B*., 2002: Determination of top-of-atmosphere longwave radiative fluxes: A comparison between two approaches using ScaRaB data. *J. Geophys. Res., 107(D8)*. ACL 6-1–ACL 6-13.

Cough, S.A., Iacono, M.J., and *Moncet, J.L.,* 1992: .Line-by-line calculations of atmospheric fluxes and cooling rates: Application to water vapor. *J. Geophys. Res. 97*, 15761–15785.

Clough, S.A., Shephard, M.W., Mlawer, E.J., Delamere, J.S., Iacono, M.J., Cady-Pereira, K., Boukabara, S., and Brown, P.D., 2005: Atmospheric radiative transfer modeling: a summary of the AER codes, Short Communication. *J. Quant. Spectrosc. RA 91*, 233–244.

Corti, T. and *Peter, T.*, 2009: A simple model for cloud radiative forcing. *Atmos. Chem. Phys. Discuss. 9*, 8541–8560.

Ebert, E.E. and *Curry, J.A.*, 1992: A parameterization of ice cloud optical properties for climate models. *J. Geophys. Res. 97(D4),* 3831–3836.

Fouquart, Y., Buriez, J.C., Herman, M., and *Kandel, R.S.*, 1990: The Influence of Clouds on Radiation: A Climate-Modeling Perspective. *Rev. Geophys. 28*, 145–166.

Fu, Q., Ping, Y., and *Sun, W.B.*, 1998: An Accurate Parameterization of the Infrared Radiative Properties of Cirrus Clouds for Climate Models. *J. Climate 11*, 2223–2237.

Geresdi, I., 1998: Idealized simulation of the Colorado hailstorm case: comparison of bulk and detailed microphysics. *Atmos. Res. 45,* 237–252.

Gettelman, A., Morrison, H., and *Ghan*, *S.J.,* 2008: A New Two-Moment Bulk Stratiform Cloud Microphysics Scheme in the Community Atmosphere Model, Version 3 (CAM3). Part II: Single-Column and Global Results. *J. Climate 21*, 3660–3679.

Harrington, J.Y., 1997: The Effects of Radiative and Microphysical Processes on Simulated Warm and Transition Season Arctic Stratus. Ph.D. Thesis, Colorado State University, Ft. Collins, CO. 298.

Harrington, J.Y., Feingold, G., and *Cotton, W.R.*, 2000: Radiative Impacts on the Growth of a Population of Drops within Simulated Summertime Arctic Stratus. *J. Atmos. Sci. 57*, 766–785.

Harrington, J. and *Olsson, P.Q.*, 2001: A method for the parameterization of cloud optical properties in bulk and bin microphysical models. Implications for arctic cloudy boundary layers. *Atmos. Res. 57,* 51–80.

Hong, G., Yang, P., Baum, B.A., Heymsfield, A.J., and *Xu, K-M.,* 2009: Parameterization of Shortwave and Longwave Radiative Properties of Ice Clouds for Use in Climate Models. *J. Climate 22*, 6287–6312.

Hongqi W. and *Gaoxiang, Z.,* 2002: Parameterization of longwave optical properties for water clouds. *Adv. Atmos. Sci. 19*, 25–34.

Hu, Y. X. and *Stamnes, K.*, 1993: An accurate parameterization of the radiative properties of water clouds suitable for use in climate models. *J. Climate 6*, 728–742.

Kunkel, B.A., 1984: Parameterization of Droplet Terminal Velocity and Extinction Coefficient in Fog Models. *J. Climate Appl. Meteorol. 23*, 34–41.

Lindner, T.H. and *Li, J.,* 2000: Parameterization of the Optical Properties for Water Clouds in the Infrared *J. Climate 13*, 1797–1805.

Liu, M., Nachamkin, J.E., and *Westphal, D.L.*, 2009: On the Improvement of COAMPS Weather Forecasts Using an Advanced Radiative Transfer Model. *Wea. Forecast 24*, 286–306.

Lynn, B.H., Khain, A.P., Dudhia, Rosenfeld, D.J., Pokrovsky, A., and *Seifert, A.*, 2005: Spectral (Bin) Microphysics Coupled with a Mesoscale Model (MM5). Part I: Model Description and First Results. *Mon. Weather Rev. 133*, 44–58.

Lynn, B. and *Khain, A.,* 2007: Utilization of spectral bin microphysics and bulk parameterization schemes to simulate the cloud structure and precipitation in a mesoscale rain event. *J. Geophys. Res. 112*, D22205.

Mitchell, D.L., 2000. Parameterization of the Mie extinction and absorption coefficients for water clouds. *J. Atmos. Sci. 57*, 1311–1326.

Mlawer, E.J., Taubman, S.J., and *Clough, S.A.*, 1995: RRTM: A Rapid Radiative Transfer Model, Fifth Atmospheric Radiation Measurement (ARM) Science Team Meeting http://www.arm.gov/publications/proceedings/conf05/extended_abs/mlawer_ej.pdf

Mlawer, E.J., Taubman, S.J., Brown, P.D., Iacono, M.J., and *Clough, S.A.,* 1997: Radiative transfer for inhomogeneous atmospheres: RRTM, a validated correlated-k model for the longwave, *J. Geophys. Res. 102(D14)*, 16663–16682.

Oreopoulos, and *L., Rossow, W.*, 2011: The cloud radiative effects of International Satellite Cloud Climatology Project weather states. *J. Geophys. Res. 116(D12202).*

Petters, J.L., Harrington, J.Y., and *Clothiaux, E.E.*, 2012: Radiative–Dynamical Feedbacks in Low Liquid Water Path Stratiform Clouds. *J. Atmos. Sci. 69*, 1498–1512.

Ramaswamy, V., Boucher, O., Haigh, J., Hauglustine, D., Haywood, J., Myhre, G., and *Solomon, S.*, 2001: Radiative forcing of climate. In *Climate Change 2001: The Scientific Basis. Contribution of Working Group I to the Third Assessment Report of the Intergovernmental Panel on Climate Change.* Cambridge, U.K.: Cambridge University Press, 349–416.

Ramanathan, V., Cess, R.D., Harrison, E.F., Minnis, P., Barkstrom, B.R., Ahmad, E., and *Hartmann, D.*, 1989: Cloud-Radiative Forcing and Climate: Results from the Earth Radiation Budget Experiment. *Science, New Series 243*, 4887, 57–63.

Ramanathan, V., Inamdar, A., 2006: The radiative forcing due to clouds and water vapor. Cambridge University Press.

Rasmussen, R.M., Geresdi, I., Thompson, G., Manning, K., Karplus, E., 2002: Freezing Drizzle Formation in Stably Stratified Layer Clouds: The Role of Radiative Cooling of Cloud Droplets, Cloud Condensation Nuclei, and Ice Initiation. *J. Atmos. Sci. 59*, 837–860.

Ritter, B., Geleyn, J.F., 1992: A Comprehensive Radiation Scheme for Numerical Weather Prediction Models with Potential Applications in Climate Simulations, *Mon. Wea. Rev. 120*, 303–325.

Roach, W.T., Slingo, A., 1979: A high resolution infrared radiative transfer scheme to study the interaction of radiation with cloud, *Q..J.Roy.Meteor.Soc. 105*, 603–614.

Rossow, W. B., Duenas, E.N., 2004: The international satellite cloud climatology project (ISCCP) web site: An online resource for research. *Bull. Amer. Meteor. Soc. 85*, 167–172.

Slingo, A., Schrecker, H.M., 1982. On the shortwave properties of stratiform water clouds. *Q. J. Roy. Meteorol. Soc. 108*, 407–426.

Stephens, G.L. 1984: The parameterization of radiation for numerical weather prediction and climate models, *Mon. Wea. Rev. 112*, 826-867.

Stephens, G.L., Tsay, S-C., Stackhouse, P.W., Flatau, P.J., 1990: The Relevance of the Microphysical and Radiative Properties of Cirrus Clouds to Climate and Climatic Feedback. *J. Atmos. Sci. 47*, 1742–1754.

Stephens, G.L., 2004: Cloud Feedbacks in the Climate System: A Critical Review. *Climate 18*, 237–273.

Straka, J.M., Kanak, K.M., and Gilmore, M.S., 2007: The behavior o f number concentration tendencies for the continuous collection growth equation using one- and two-moment bulk parameterization schemes. *J. Appl. Meteorol. Climatol. 46*, 1264–1274.

Tompkins, A.M. and Di Giuseppe, F., 2009: Cloud radiative interactions and their uncertainty in climate models, in P. Williams and T. Palmer, eds., Stochastic Physics and Climate Models, *Cambridge University Press, UK*

Tzivion, S., Feingold, G. Levin, Z., 1987: An efficient numerical solution to stochastic collection eqation, *J. Atmos. Sci. 44*, 3139–3149.

Walko, R.L., Cotton, W.R., Meyers, M.P., Harrington, J.Y., 1995: New RAMS cloud microphysics parameterization: Part I. The single moment scheme. *Atmos. Res. 38*, 29–62.

Wielicki, B.A., Barkstrom, B.R., Harrison, E.F., Lee, R.B., Smith, G.L., and Cooper, J.E., 1996: Clouds and the earth's radiant energy system (CERES): An earth observing system experiment. *B. Am. Meteorol. Soc. 77*, 853–868.

Appendix A

Q_{ext} depends on the droplet diameter (D), wavelength (λ), and index of refraction (m), with the imaginary component n_i and real component n_r:

$$Q_{ext}(D, \lambda, m) = 2K(tD), \tag{A1}$$

where $t = \frac{2\pi}{\lambda}[n_i + i(n_r - 1)]$, $m = n_r - i \times n_i$, and $K(x) = 1 + 2\text{Re}\left[\frac{e^{-x}}{x} + \frac{e^{-x} - 1}{x^2}\right]$.

The correction parameter C_{res} is a rather complicated function of the drop size and the refraction index:

$$C_{res} = r_a \frac{k^m e^{-\varepsilon k}}{k_{max}^m e^{-m}}, \tag{A2}$$

where

$$r_a = 0.7393 n_r - 0.6069, \tag{A3}$$

and

$$m = \frac{1}{2}, \quad k = \frac{D}{\lambda}, \quad k_{max} = \frac{m}{\varepsilon}, \text{ and } \varepsilon = \frac{1}{4} + 0.6\{1 - \exp[-\frac{8\pi n_i}{3}]\}^2. \tag{A4}$$

The Q_{edge} term in Eq.(1) is given by:

$$Q_{edge} = 2(\pi k)^{-2/3}[1 - \exp(-0.06\pi k)]. \tag{A5}$$

After substituting Eqs. (A1)–(A5) into Eq. (1) or Eq. (7), we can evaluate the extinction efficiency as a function of droplet diameter, wavelength, and refraction index (which is the $Q_{ext}(D, \lambda, m)$ function in explicit form).

Appendix B

Using the MADT method Eq. (8), the integral in Eq. (7) can be divided in three parts:

$$\beta_{ext,i}= \sum_{j=1}^{16} \sum_{k=2}^{N_{bins}} [\int_{\Delta\lambda_j} (E_\lambda \int_{M_{k-1}}^{M_k} A(D)Q_{ext,i}(D,m,\lambda)n_k(M)dM\,d\lambda)/\int_{\Delta\lambda_j} E_\lambda d\lambda]$$, (B1)

where

$$Q_{ext,1}(D,\lambda,m)= Q_{ext} , \quad Q_{ext,2}(D,\lambda,m)= \frac{C_{res}}{2}\times Q_{ext} , \text{ and } Q_{ext,3}(D,\lambda,m)= Q_{edge} ,$$

and *j* is the number of band in *Table 1*. Using the appropriate equations from the Appendix A, the above integral can be written as the sum of the next three equations. After substitution of Eq. (6) in (B1), the integrals can be evaluated analytically.

$$\beta_{ext,1}= \sum_{j=1}^{16} \sum_{k=2}^{N_{bins}} [\int_{\Delta\lambda_j} (E_\lambda \int_{M_{k-1}}^{M_k} (\frac{\pi}{4}\times D^2(1+2\mathrm{Re}[\frac{e^{-tD}}{tD}+\frac{e^{-tD}-1}{t^2 D^2}]))(A_k+M\times B_k)dM\,d\lambda)/\int_{\Delta\lambda_j} E_\lambda d\lambda]=$$

$$=\sum_{k=2}^{N_{bins}} A_k\times \sum_{j=1}^{16} K_{A1kj}(M_{k-1},M_k,\Delta\lambda_j)+\sum_{k=2}^{N_{bins}} B_k\times \sum_{j=1}^{16} K_{B1kj}(M_{k-1},M_k,\Delta\lambda_j)$$.

$$\beta_{ext,2}= \sum_{j=1}^{16} \sum_{k=2}^{N_{bins}} [\int_{\Delta\lambda_j} (E_\lambda \int_{M_{k-1}}^{M_k} (\frac{\pi}{4}\times D^2(1+2\mathrm{Re}[\frac{e^{-tD}}{tD}+\frac{e^{-tD}-1}{t^2 D^2}])\times \frac{C_{res}}{2}\times (A_k+M\times B_k)dM\,d\lambda)/\int_{\Delta\lambda_j} E_\lambda d\lambda]=$$

$$=\sum_{k=2}^{N_{bins}} A_k\times \sum_{j=1}^{16} K_{A2kj}(M_{k-1},M_k,\Delta\lambda_j)+\sum_{k=2}^{N_{bins}} B_k\times \sum_{j=1}^{16} K_{B2kj}(M_{k-1},M_k,\Delta\lambda_j)$$.

$$\beta_{ext,3}= \sum_{j=1}^{16} \sum_{k=2}^{N_{bins}} [\int_{\Delta\lambda_j} (E_\lambda \int_{M_{k-1}}^{M_k} (\frac{\pi}{4}\times D^2\times 2(\pi\frac{D}{\lambda})^{-\frac{2}{3}}[1-e^{-0.06\pi\frac{D}{\lambda}}](A_k+M\times B_k)dM\,d\lambda)/\int_{\Delta\lambda_j} E_\lambda d\lambda]=$$

$$=\sum_{k=2}^{N_{bins}} A_k\times \sum_{j=1}^{16} K_{A3kj}(M_{k-1},M_k,\Delta\lambda_j)+\sum_{k=2}^{N_{bins}} B_k\times \sum_{j=1}^{16} K_{B3kj}(M_{k-1},M_k,\Delta\lambda_j)$$.

The final K_{Akj} and K_{Bkj} kernels are the sum of the K_{ikj} constants in the three parts (*i*=1,2,3).